Arch. Metall. Mater. **71** (2026), 1, 361-374

DOI: https://doi.org/10.24425/amm.2026.157799

Y.J. SHI[1,2], F.J. LI[3*], Z.Y. CHEN[2], Y.H. ZHAN[2], L.M. QIAN[5], M. LIU[4], X. ZHOU[3]

EFFECTS OF HEAT TREATMENT ON THE CORROSION BEHAVIOR AND MECHANICAL PROPERTIES OF SiCp/Al-Mg-Si-Cu MATERIALS

This study investigates the effects of solution and aging heat treatments on SiCp/Al-Mg-Si-Cu aluminum matrix composites using scanning electron microscopy, confocal microscopy, salt spray corrosion tests, and electrochemical characterization. Solution and aging treatments promote finely dispersed $CuMgA_2$ phases, significantly enhancing mechanical properties, increasing hardness to 134 HV and strength to 440 MPa. With prolonged corrosion, particle stripping on the composite surface intensifies. After 8 days of corrosion, morphology fluctuation variances are 14.40 for untreated samples, 5.73 for solution-treated samples, and 4.40 for aged samples. Electrochemical tests reveal that aged samples have the lowest corrosion current (1.616×10^{-7} A/cm^2) and the largest capacitive arc, indicating superior corrosion resistance. XPS analysis confirms that aging results in uniformly distributed $CuMgAl_2$ phases, enhancing corrosion resistance. Aging treatment significantly improves corrosion resistance, followed by solution treatment, with untreated samples performing the worst.

Keywords: Aluminum Matrix Composites; Aging Heat Treatment; Corrosion Behavior; Mechanical Properties

1. Introduction

Aluminum matrix composites are essential materials in industries such as aviation, automotive, and marine due to their unique combination of properties. These composites exhibit high specific strength, high specific modulus, excellent thermal conductivity, and a low thermal expansion coefficient, making them highly desirable for advanced applications [1-4]. Additionally, their superior service performance has established them as a research focus in the field of advanced composites. Notably, aluminum matrix composites are widely used in the construction of hulls and critical components for ships and offshore structures, where prolonged exposure to high-salinity seawater demands exceptional corrosion resistance. This capability not only extends the service life of these structures but also significantly reduces maintenance costs [5].

Relevant studies have shown that appropriate heat treatment processes significantly affect the mechanical properties of aluminum matrix composites [6]. Specifically, Ma et al. investigated the aging strengthening mechanism of Al-Zn-Mg-Cu composites and proposed that a T6 heat treatment process involving aging at 120°C for 24 h can significantly optimize the aging kinetics of the material. Compared to conventional artificial aging, this process allows the alloy to reach its peak hardness (238 HV) 14 h earlier, with a 29 HV increase over the non-reinforced alloy. This enhancement is attributed to the solution treatment at 500-540°C, which facilitates the complete dissolution of soluble phases in the matrix and the formation of a uniform supersaturated solid solution. Subsequent aging treatment significantly strengthens the reinforcing effect of SiC particles via dislocation modulation mechanisms. The mismatch in thermal expansion coefficients between SiC particles and the aluminum matrix induces a high density of dislocations during quenching, which promotes the precipitation of η' phase during aging, thereby enhancing the mechanical properties of the composite after heat treatment [7]. Additionally, Zhu et al. conducted a comparative study on the influence of Cu addition on the natural aging behavior of SiC/Al-Mg-Si-Cu composites. Compared with composites without Cu, those with Cu exhibited a decrease in yield strength from 541 MPa to 462 MPa (a reduction of 73 MPa) after one week of

[1] NANJING UNIVERSITY OF INFORMATION SCIENCE AND TECHNOLOGY, SCHOOL OF ELECTRONICS AND INFORMATION ENGINEERING, NANJING, P.R. CHINA
[2] NANJING UNIVERSITY OF INDUSTRY TECHNOLOGY, INDUSTRIAL PERCEPTION AND INTELLIGENT MANUFACTURING EQUIPMENT ENGINEERING RESEARCH CENTER OF JIANGSU PROVINCE, NANJING, P.R. CHINA
[3] SHANGHAI UNIVERSITY OF ENGINEERING SCIENCE, SCHOOL OF MATERIALS SCIENCE AND ENGINEERING, SHANGHAI, P.R. CHINA
[4] SHANGHAI INSTITUTE OF TECHNOLOGY, SCHOOL OF MATERIALS SCIENCE AND ENGINEERING, SHANGHAI, P.R. CHINA
[5] NANTONG INSTITUTE OF TECHNOLOGY, SCHOOL OF MECHANICAL ENGINEERING, NANTONG, P.R. CHINA

* Corresponding author: fangjieli119@126.com

natural aging, while the elongation increased from 9% to 12%. Notably, after two weeks of natural aging, the yield strength of the composites remained stable, whereas the unreinforced alloy showed a strength reduction of approximately 6%. Therefore, for such aluminum matrix composites, both solution and aging heat treatments play a critical role in enhancing their mechanical properties [8-9].

Aluminum matrix composites have been extensively studied due to their potential to enhance mechanical properties and corrosion resistance through tailored microstructures and heat treatment processes. Singh et al. [10] conducted electrochemical tests on silicon carbide particle-reinforced aluminum matrix composites with mass fractions of 10%, 15%, and 25%. The results indicated that the composite with a 10% SiC mass fraction exhibited the best corrosion resistance. Beyond this threshold, corrosion resistance decreased due to crack formation, which accelerated corrosion along these cracks. The increased SiC particle volume fraction also created numerous interfaces in the composite, forming corrosion channels that accelerated degradation and reduced corrosion potential. Zakaria et al. [11] investigated the corrosion resistance of SiCp/Al composites with varying SiC particle sizes (3 μm, 6 μm, and 11 μm) at a constant volume fraction of 15%. Their study found that the corrosion rate decreased as the particle size increased, attributing this to the galvanic action of intermetallic precipitates, which reduced the composite's overall corrosion resistance. Xiao et al. [12] employed the Exfoliation test and Potentiodynamic polarization tests to investigate the corrosion behavior of Al-Zn-Mg-Cu-Zr-Sc alloys in different tempering states. The study revealed that due to the discontinuous distribution of the η phase at grain boundaries, overaging reduced the alloy's susceptibility to exfoliation corrosion, causing a negative shift in the corrosion potential. Additionally, the Al-Zn-Mg-Cu-Zr-Sc alloys showed enhanced resistance to exfoliation corrosion after aging treatment. Xie et al. [13] used deformation-driven metallurgy to prepare graphene nanoplatelets (GNPs) to enhance aluminum matrix composites, providing long-term corrosion resistance. Severe plastic deformation achieved uniform dispersion of GNPs and grain refinement, inhibiting the formation of pores and hydrolyzable compounds, thus preventing crevice corrosion. The GNP-containing protective oxide film reduced the corrosion rate. Experimental and computational results indicated that the synergistic effect of GNPs and the oxide film formed a carbon-doped protective film, significantly improving the composite's corrosion resistance and delaying chloride ion penetration and charge transfer. M. Suśniak et al. [14] found that for AlSi5Cu2 matrix composites containing 10, 15, and 20 wt.% SiC particles, as the SiC content increased, the hardness and stress values of the composites significantly improved, but the ductility decreased. Wang *e*t al. [15] performed salt spray tests on 2024 aluminum matrix and WCp/2024 composites, observing that while the aluminum matrix surface developed randomly distributed corrosion pits, WC particles acted as inert barriers, preventing significant pitting. In contrast, Al-B4C composites were more prone to pitting corrosion due to oxygen diffusion and galvanic coupling between the matrix and reinforcement [16].

The unique thermal conductivity of SiC particles in aluminum matrix composites makes traditional aluminum alloy heat treatment processes less effective. Aval et al. [17] studied the effects of artificial aging heat treatment on Al-Zn-Mg-Cu-based composites, reporting a 24% increase in shear strength and a 13% increase in hardness, but a 39% decrease in corrosion resistance. Kumar et al. [18] investigated the performance changes of aluminum alloys and their composites after aging heat treatment through microstructural analysis and mechanical performance testing.The study revealed that the 7XXX series alloys, using the double aging > RR > T6 conditions method to address SCC retrogression and re-aging issues, improved stress corrosion cracking resistance and hardness via precipitation hardening treatment, although ductility and ultimate tensile strength were slightly reduced. Wang et al. [19] utilized microstructural analysis and mechanical property tests to investigate the effects of heat-treated TiB_2 particles on the mechanical properties of AL-3.5Cu-1.5Mg-1Si composites. The study revealed that after T6 heat treatment, the Q phase disappeared, forming Al_xMn_y, Mg_2Si, and $Al_2Cu(Mg)$ phases. Compared to the non-reinforced A-Cu-Mg-Si alloy, the heat-treated TiB_2/AL-Cu-Mg-Si composites exhibited significantly refined grains, thus enhancing their mechanical properties. Hao et al. [20] demonstrated that TiB_2 particles accelerated aging precipitation in 7055 aluminum matrix composites, significantly enhancing hardness and tensile strength under optimal conditions (460°C solution treatment for 60 minutes, followed by aging at 120°C for 20 hours). Similarly, Shang et al. [21] reported improvements in tensile strength (320 MPa), yield strength (244 MPa), elongation (6.91%), and microhardness (114 HV) in SiCp/ZL101 composites after solution and aging treatments. Wang et al. [22] investigated the effects of T6 heat treatment on the mechanical properties of selective laser melted AlSi10Mg aluminum alloy through microstructural analysis and mechanical property tests. The experiments demonstrated that after solution treatment, the tensile strength slightly decreased by 19.97%, while the elongation significantly increased by up to 155%. The bending strength slightly decreased by 6.1%, whereas the fracture toughness significantly increased by up to 122.9% after T6 heat treatment. The study indicated that due to the spheroidization and diffusion of silicon precipitates during the T6 heat treatment, the alloy's plasticity and ductility were improved without causing significant impacts on the tensile and bending strengths. Zhang et al. [23] found that aging treatment improved the strength and ductility of particle-reinforced composites, with optimal tensile strength (309 MPa), yield strength (240 MPa), and elongation (3.7%) achieved after 10 hours of aging. Lei et al. [24] demonstrated that higher solution temperatures for 6013 aluminum alloy enhanced tensile strength, microhardness, and corrosion resistance after T6 aging, though elongation and conductivity decreased. The improvements were attributed to increased GP zones and L phases, along with a reduction in grain boundary precipitates, which reduced intergranular corrosion. Similarly, Liu et al. [25] found that double aging treatments for 7075 aluminum alloy eliminated interlayer structures, dispersed T phases, and enhanced hardness and corrosion resistance.

By optimizing heat treatment processes and controlling the morphology, size, and distribution of precipitates, the key properties of aluminum matrix composites – such as mechanical strength and corrosion resistance – can be significantly enhanced. This study investigates the effects of different heat treatment processes on the microstructure, surface morphology, and polarization curves of SiCp/Al-Mg-Si-Cu composites, providing experimental insights and a theoretical basis for selecting optimal processing conditions for aluminum matrix composites.

2. Experimental

2.1. Materials and heat treatment process

The experimental material in this study is based on a commercially available aluminum matrix composite provided by a company. The matrix is an Al-Mg-Si-Cu alloy, and the reinforcement phase consists of irregularly shaped SiC particles. The composite was fabricated using a combination of powder metallurgy and hot extrusion processes, with the specific steps as follows:

First, the matrix alloy powder (particle size ≤50 μm) and SiC particles (density: 3.21 g/cm^3, melting point: 2300°C, D50 = 15 μm) were uniformly mixed via ball milling at a ball-to-powder ratio of 3:1, a rotation speed of 200 rpm, and a milling duration of 2 hours. Next, the mixed powder was cold-pressed under argon protection at a pressure of 400 MPa. The cold-pressed compact was then subjected to vacuum hot-press sintering at 580°C under a pressure of 30 MPa, with a holding time of 1 hour. Finally, the sintered billet underwent hot extrusion at 480°C with an extrusion ratio of 10:1 to obtain rod-shaped specimens.The alloy composition was determined using inductively coupled plasma optical emission spectroscopy (ICP), as shown in TABLE 1. Statistical analysis of the metallographic samples using Image-Pro Plus software confirmed that the SiC volume fraction was 16 ±0.8%, with the particles exhibiting a dispersed distribution.

TABLE 1

Composition of Al-Mg-Si-Cu alloy (mass fraction)

Element	Mg	Mn	Si	Cu	Fe	Trace element	Al
Mass fraction (%)	3.40	0.42	0.75	0.94	0.25	0.16	rest

To explore the effects of solution and aging heat treatment processes on the microstructure and mechanical properties of SiCp/Al-Mg-Si-Cu composites, a vacuum tube high-temperature sintering furnace (model OFT-1200X) was utilized. This furnace can reach a maximum temperature of 1200°C with ±1°C control accuracy, During the solution treatment, the specimen was placed in a quartz tube with a flow of high-purity argon gas (15 L/min). After being held at 520°C for 3 hours, the specimen was rapidly transferred (<5 s) to a water bath at room temperature (20 ±2°C) to complete quenching. The aging treatment was carried out by holding the specimen at 160°C in the furnace for 5 hours, followed by air cooling,offering multi-segment temperature regulation via PID control and the option to introduce inert gases. As shown in Fig. 1, the optimized heat treatment process for the SiCp/Al-Mg-Si-Cu composite studied in this paper consists of a solution treatment at 520°C for 3 hours followed by water quenching, followed by an aging treatment at 160°C for 5 hours.

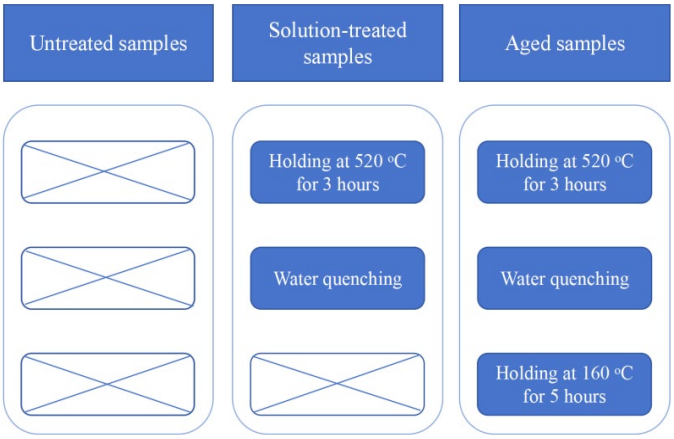

Fig. 1. Heat treatment experimental scheme of SiCp/Al-Mg-Si-Cu composite

2.2. Microstructural characterization

Samples were prepared using metallographic embedding material, followed by grinding and polishing. Afterward, they were cleaned and dried before being treated with Keller's reagent for 20-25 seconds, washed with running water and ethanol, and blow-dried. Microstructural observations were conducted using a Hitachi S4800 scanning electron microscope (SEM) equipped with energy-dispersive spectroscopy (EDS). This SEM achieves electron imaging precision within 1 nm and was used for point and area scans of compositional changes at various magnifications. Images were processed uniformly for analysis.

For phase characterization, samples were cut using a wire cutting machine, embedded, ground with 800#, 1500#, and 2000# sandpapers, and polished with a 1.0 grit polishing agent. A D/Max2500V X-ray diffractometer with a Cu-Kα target (λ = 1.541 Å) was used, operating at 40 mA current, 5°/min scanning speed, and a diffraction angle range of 20°-100°.

To analyze the valence states of elements in the passivation film after different heat treatments, a Thermo Scientific K-Alpha+ X-ray photoelectron spectrometer (XPS) was employed. Samples (less than 5 mm in length and width, and 3 mm in height) were polished, ultrasonically cleaned, and coated before testing. C 1s (284.8 eV) was used as the standard for spectrum calibration, and peak fitting was performed using Advantage software. The data were subsequently visualized using Origin software.

For salt spray corrosion experiments, a LEXT OLS5000 confocal microscope was used to characterize the three-dimensional morphology of sample surfaces after exposure. Samples were positioned level under the objective lens to ensure flatness,

and appropriate magnifications were selected to obtain detailed morphology maps. The corrosion depth change curves were analyzed, and the results were visualized using Origin software.

2.3. Mechanical property testing

The hardness testing of the samples was conducted using an HXD-1000TMC Vickers microhardness tester. Prior to testing, the samples were ground and polished to a finish exceeding 2000#. A load of 200 gf was applied for 10 seconds. Hardness was measured at ten different positions using the cross-sectional measurement method, and the average value was determined. The test conditions followed the national standard for metal material tensile testing, GB/T 228.1-2010. Tensile testing of the 2.5 mm thick SiCp/Al-Mg-Si-Cu composites was carried out using an LD23.503 universal testing machine. Samples were machined into a dumbbell shape with dimensions of 45 mm × 10 mm as shown in Fig. 2 and polished to a finish exceeding 2000#. Each group of specimens was subjected to five tensile tests with a strain rate of 1×10^{-3} s^{-1}. The resulting data were used to plot stress-strain curves.

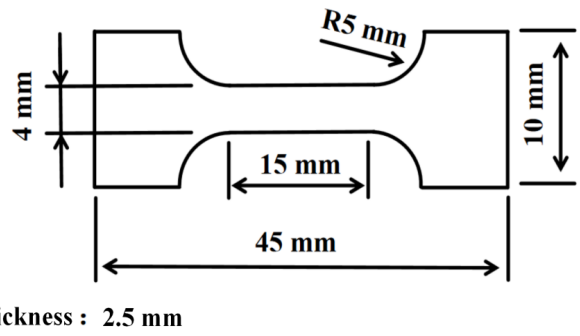

Fig. 2. Tensile specimens and dimensions of SiCp/Al-Mg-Si-Cu

2.4. Corrosion resistance testing

The salt spray test was conducted in accordance with ASTM B117-19 using a BGD 881 salt spray chamber. Prior to testing, the specimens were sequentially ground with 800#, 1500#, and 2000# sandpaper, polished, and ultrasonically cleaned in deionized water and ethanol, followed by drying. The salt solution was prepared with 3.5 wt.% NaCl (analytical grade, purity ≥99.8%, pH = 6.8 ±0.1) and allowed to stand for 24 h before use. The test conditions were maintained at a chamber temperature of 35 ±1°C, a saturation tower temperature of 47 ±1°C, and a relative humidity of ≥ 95%. The spray rate was controlled at 1.5 ±0.2 mL/(h·80 cm^2) using a peristaltic pump (BT100-1F) for quantitative replenishment. The specimens were placed at an angle of 20° ±2° to the vertical to avoid direct droplet impact. The pH of the condensate was monitored every 24 h using a Mettler Toledo FE28 pH meter (accuracy ±0.02). After exposure for 4, 6, or 8 days, the specimens were removed, gently rinsed with deionized water to remove residual salt crystals, and then immersed in a 70°C chromic-phosphoric acid solution (200 g/L CrO_3 + 10 g/L H_3PO_4) for 10 min to remove corrosion products. Finally, the specimens were dehydrated with ethanol and dried with cold air.

Electrochemical tests were conducted using a Chenhua CHI660D electrochemical workstation, following the GB/T 40299-202 standard for corrosion testing of metals and alloys. A 3.5% sodium chloride solution was prepared with a purity greater than 99%. A three-electrode system was used, with the sample as the working electrode, a platinum electrode as the counter electrode, and a saturated calomel electrode (SCE) as the reference.

3. Results

3.1. Microstructural evolution

To investigate the evolution of SiCp/Al-Mg-Si-Cu composites during the solution-aging process, their microstructure and mechanical properties were characterized in three states: untreated (marked as untreated samples), peak solution-treated (marked as solution-treated samples), and peak-aged (marked as aged samples). XRD patterns of all three sample types, presented in Fig. 3, revealed characteristic peaks for Al (JCPDS 89-3657), SiC (JCPDS 72-0018), and $CuMgAl_2$ (JCPDS 65-2504) phases [26]. Notably, no oxidation peaks were detected, indicating that the sample surfaces were free of oxidation and that the sample quality was excellent. The lattice parameters of the Al phase, calculated using the Bragg equation, are summarized in TABLE 2. The lattice parameters increased from 4.0413 Å (untreated) to 4.0459 Å (solution-treated) and then decreased to 4.0416 Å (aged), indicating that a supersaturated solid solution formed during solution treatment, followed by precipitation of phases during the aging process [27,28]. These results suggest that the phase structure of SiCp/Al-Mg-Si-Cu composites can be effectively tailored by controlling the heat treatment process.

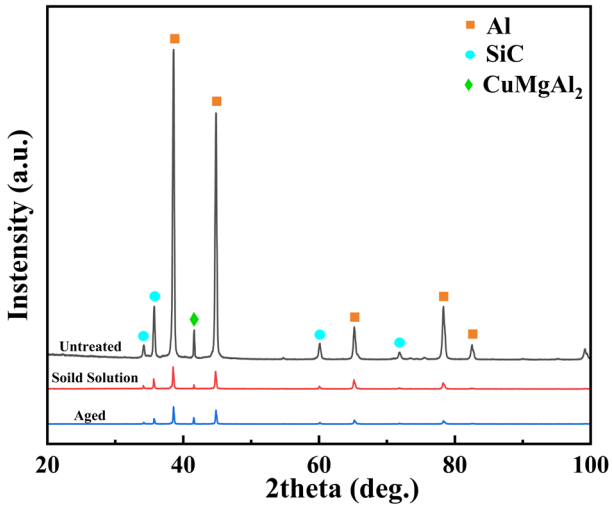

Fig. 3. XRD patterns of SiCp/Al-Mg-Si-Cu composite with different heat treatments

TABLE 2

The lattice parameters of the Al phases in the different samples

Specimen status	Lattice constant (Å)
Untreated	4.0413
Solid Solution state	4.0459
Aged state	4.0416

The microstructure and elemental distribution of untreated, solution-treated, and aged samples, as shown in Fig. 4, revealed a uniform distribution of SiC particles within the matrix. Additionally, the presence of Al, Mg, and Cu elements confirmed the formation of the $CuMgAl_2$ intermetallic compound (Fig. 4(d)). In untreated samples, numerous fine $CuMgAl_2$ phases were observed (Fig. 4(a)). After solution treatment, the quantity of these fine phases decreased (Fig. 4(b)). In aged samples, SEM images (Fig. 4(c)) showed larger and more abundant $CuMgAl_2$ phases, resulting from the coarsening and precipitation of these phases during aging. The addition of SiC particles, along with the precipitation of $CuMgAl_2$ phases, was found to accelerate aging kinetics by acting as nucleation agents. Consequently, it can be inferred that, in addition to the reinforcement provided by SiC particles, the precipitation strengthening effect of the $CuMgAl_2$ phase plays a critical role in enhancing the overall mechanical properties of the composite [29-31].

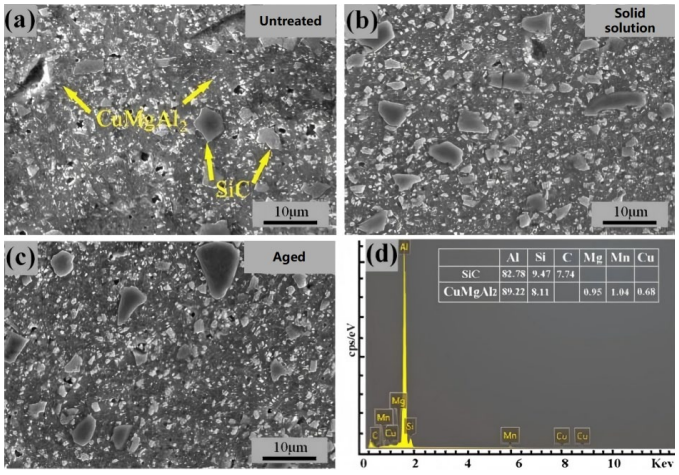

Fig. 4. SEM microstructure of SiCp/Al-Mg-Si-Cu composites with different heat treatments (a) Untreated state (b) Soild Solution state (c) Aged state microforms (d) and their energy spectra

3.2. Mechanical properties

Fig. 5 presents the mechanical properties of the SiCp/Al-Mg-Si-Cu composite under different heat treatment conditions. It can be observed that the hardness of the untreated specimen is 132 HV. After solution treatment at 520°C for 3 hours, the hardness decreases to approximately 124 HV, showing a reduction of 6.1%. After aging at 160°C for 5 hours, the hardness slightly increases to about 134 HV. Compared to the untreated specimen, the hardness in the aged condition increases by 1.5%, while compared to the solution-treated specimen, it increases by 8.1%.

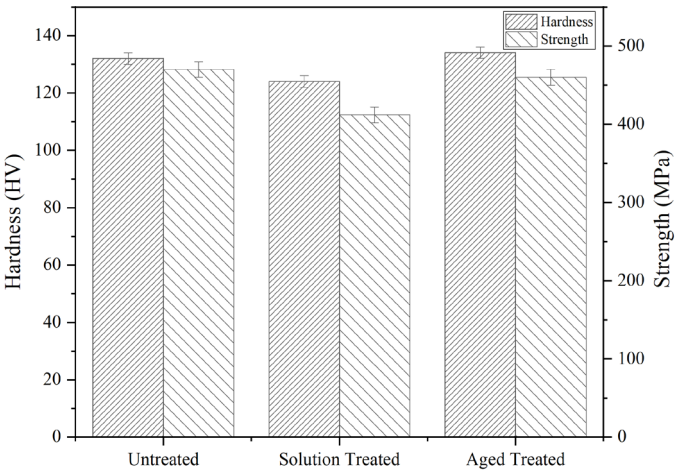

Fig. 5. Mechanical properties of SiCp/Al-Mg-Si-Cu composites under different heat treatment processes

Additionally, Fig. 5 shows that the untreated specimen has a tensile strength (UTS) of 473 MPa and an elongation (EL) of 5.1%. After solution treatment at 520°C for 3 hours, the strength decreases to 412 MPa, with an elongation of 6.2%, resulting in a 13% reduction in strength. After aging at 160°C for 5 hours, the composite's strength recovers to 470 MPa with an elongation of 5.2%. Compared to the solution-treated specimen, it increases by 14.1%.

The observed changes in mechanical properties can be explained by the microstructural evolution during heat treatment. During solution treatment, precipitated phases dissolve into the aluminum matrix, forming a supersaturated solid solution. This process homogenizes the alloy composition but reduces the strengthening effect of the precipitates, leading to lower hardness and strength in the solution-treated samples. In contrast, aging facilitates the precipitation of fine strengthening particles, which impede dislocation movement through a "pinning" effect. This results in partial recovery of hardness and strength after aging treatment [32].

3.3. Salt spray corrosion behavior

Fig. 6 presents the surface morphology of untreated, solution-treated, and aged SiCp/Al-Mg-Si-Cu composite samples after varying durations of salt spray corrosion. For the untreated sample, corrosion traces began to appear after 4 days of exposure, as shown in Fig. 6(a). By 6 days, rust spots and the corroded area on the surface had significantly increased, as illustrated in Fig. 6(b). After 8 days, the sample surface was almost entirely corroded, as seen in Fig. 6(c). The results indicate that both the extent of the corroded area and the severity of corrosion intensified with increasing exposure time.

A comparison of the three sample types under identical exposure durations highlights clear differences in corrosion resistance. After 4 days of corrosion, aged samples exhibited the smallest and least numerous corrosion spots, solution-treated

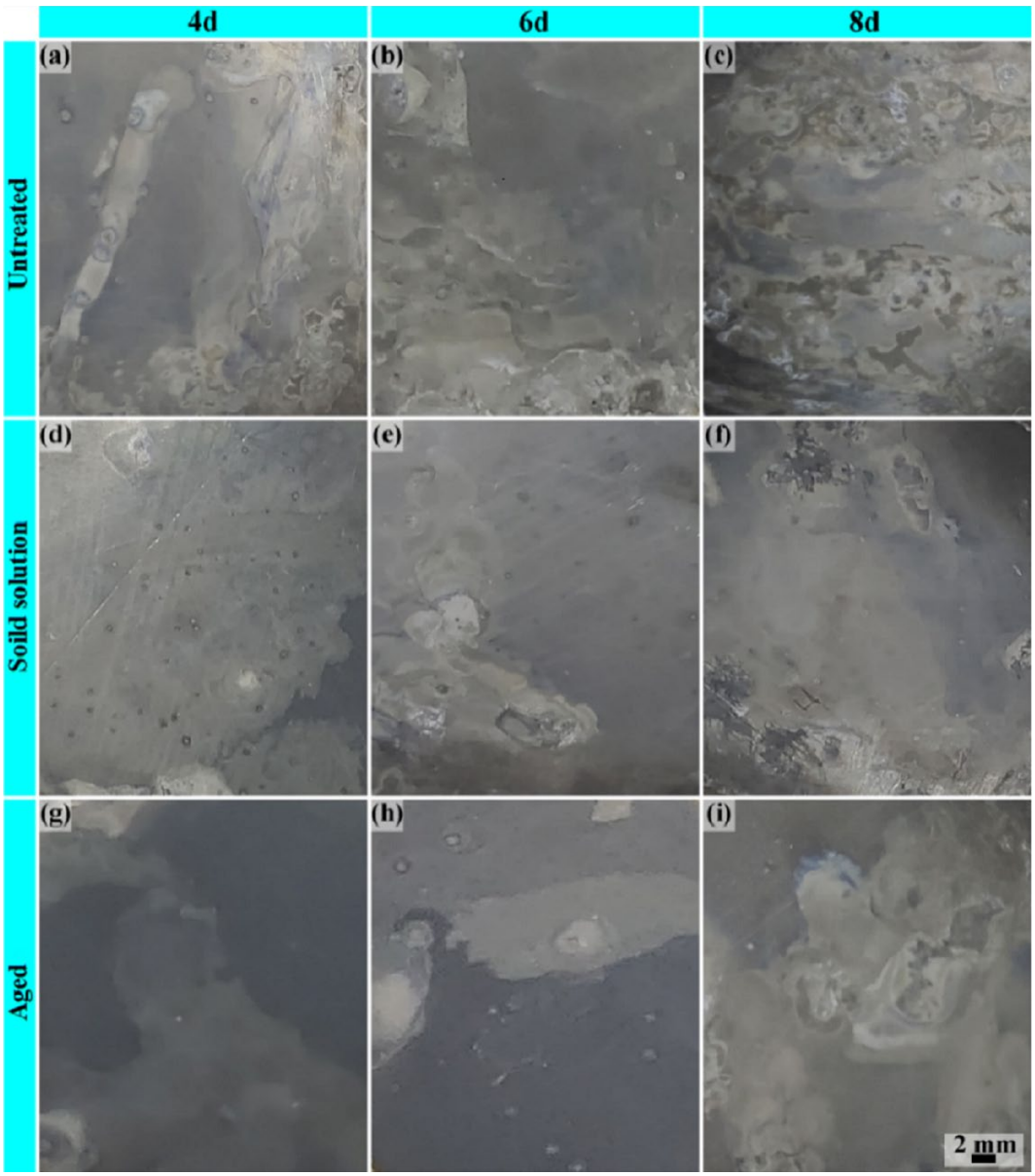

Fig. 6. Photomicrographs of the surface of Untreated, Soild Solution sample and Aged samples after salt spray corrosion for different times

samples showed moderate corrosion, and untreated samples experienced the most significant damage. This trend persisted as corrosion time increased, with untreated samples displaying the largest pitting corrosion, followed by solution-treated samples, and aged samples exhibiting the smallest pits and least surface damage.

These observations demonstrate that aging treatment provides the highest resistance to salt spray corrosion, primarily due to the formation of fine and uniformly distributed $CuMgAl_2$ phases, which enhance surface compactness and reduce the penetration of corrosive media. Solution treatment moderately improves corrosion resistance by forming a more uniform solid solution, although it lacks the protective effect of the precipitates formed during aging. In contrast, untreated samples, which lack phase precipitation and surface strengthening, are the most susceptible to corrosion, showing extensive damage and deep pitting over time.3.4 Electrochemical characteristic analysis.

3.4. Electrochemical characteristic analysis

3.4.1. Polarization curve analysis

Fig. 7 shows the potentiodynamic polarization curves of untreated, solution-treated, and aged samples. By comparing the polarization curves of the three samples, it can be observed that their shapes are similar, indicating consistent electrochemical reactions in the anode and cathode regions, and no significant passivation behavior was observed. This suggests that under the experimental conditions used, the corrosion mechanisms of the three samples do not significantly differ. To further analyze corrosion performance, the electrochemical parameters obtained from fitting the polarization curves were extracted and displayed in the graph. From the fitting results, the corrosion potentials (*Ecorr*) of the three samples [33] are not significantly different. The corrosion potential of the untreated sample is –714 mV,

the solution-treated sample is –679 mV, and the aged sample is –718 mV. In terms of corrosion current density (*Icorr*), the aged sample has an Icorr of 1.616×10^{-7} A/cm^2, the solution-treated sample has 5.573×10^{-7} A/cm^2, and the untreated sample has 1.537×10^{-6} A/cm^2. The Icorr value directly reflects the corrosion rate of the material; a smaller Icorr indicates superior corrosion resistance. Therefore, the aged sample has the lowest corrosion rate, showing the best corrosion resistance, followed by the solution-treated sample, while the untreated sample has the highest corrosion rate and the poorest corrosion resistance.

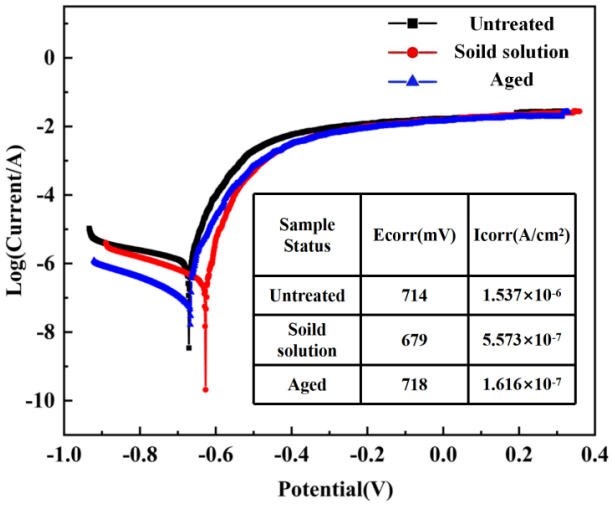

Sample Status	Ecorr(mV)	Icorr(A/cm²)
Untreated	714	1.537×10⁻⁶
Soild solution	679	5.573×10⁻⁷
Aged	718	1.616×10⁻⁷

Fig. 7. Polarization curves of Untreated sample, soild solution sample and aged sample

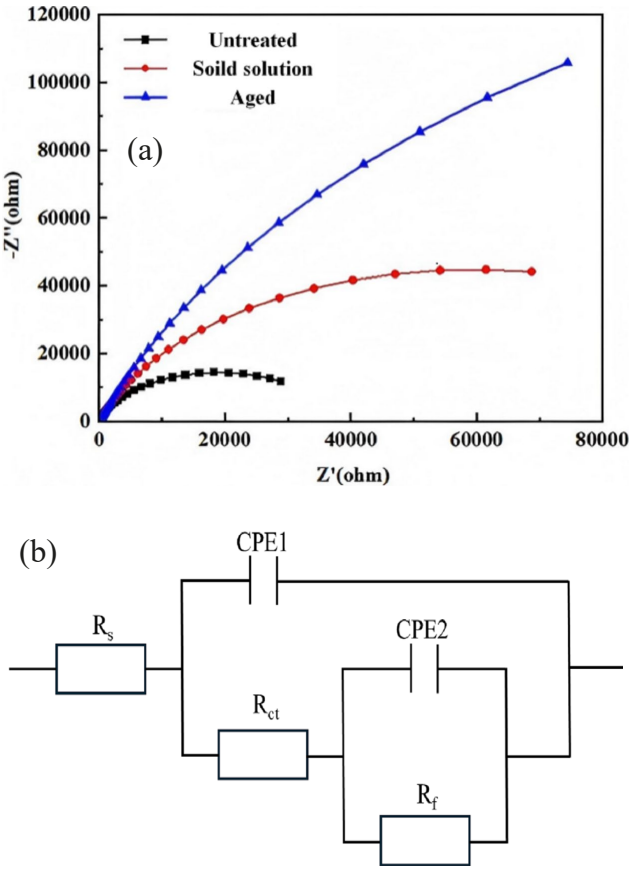

Fig. 8. (a) Electrochemical AC impedance profiles of Untreated sample, soild solution sample and aged sample; (b) Equivalent circuit model

In summary, the analysis of the above results leads to the conclusion that the corrosion resistance of aged composites is superior to that of solution-treated composites, and the corrosion resistance of solution-treated composites is superior to that of untreated composites. This indicates that aging treatment can significantly improve the corrosion resistance of aluminum alloy composites, surpassing the performance of materials that are only solution-treated or untreated.

3.4.2. AC Impedance spectroscopy analysis

Fig. 8(a) displays the AC impedance spectra of untreated, solution-treated, and aged SiCp/Al-Mg-Si-Cu composite samples. In the high-frequency region, all three sample types exhibit a capacitive arc, with semicircular curves representing the impedance characteristics of the material. The real part (Z') corresponds to the charge transfer resistance, while the imaginary part ($-Z''$) represents the capacitive behavior of the material. A larger arc radius indicates higher charge transfer resistance (*Rct*), which reflects improved corrosion resistance [34]. As shown in the figure, both Z' and $-Z''$ increase for the aged samples, suggesting greater resistance to charge transfer and superior corrosion protection.

The results are consistent with the findings from the salt spray corrosion tests, further confirming the enhanced corrosion resistance of aged samples. The AC impedance spectra were analyzed using the equivalent circuit model shown in Fig. 8(b). In this model: *Rs* represents the solution resistance, *Rct* denotes the charge transfer resistance, *Rf* indicates the resistance of the passive film, *CPE*1 corresponds to the electrochemical double-layer capacitance, and *CPE*2 represents the passive film capacitance.

To account for the uneven surface morphology and energy dissipation of the electrode, a constant phase element (*CPE*) was introduced to simulate the capacitive behavior of the material more accurately. The impedance of the constant phase element (Q) is defined by the following formula:

$$Z_Q = \frac{1}{Y_0}(j\omega)^{-n} \tag{1}$$

Where: j is the imaginary unit ($j^2 = -1$), ω is the angular frequency ($\omega = 2\pi f$), Y_0 is the *CPE* constant, and n ($-1 < n < 1$) is the phase angle exponent, which describes the deviation from ideal capacitive behavior.

The larger arc radius and higher charge transfer resistance observed in the aged samples confirm their superior corrosion resistance, attributable to the formation of a compact and stable passive film. Conversely, untreated and solution-treated samples exhibit smaller arc radii, indicating less effective resistance to charge transfer and poorer corrosion resistance.

3.4.3. XPS analysis

The X-ray photoelectron spectroscopy (XPS) analysis was conducted to evaluate the surface composition and chemical bonding states of the aged samples. As shown in Fig. 9, the Al 2p peak located at 73.5 eV indicates the presence of Al_2O_3 and $Al(OH)_3$. In the Cl 2p spectrum, peaks at 197.4 eV and 198.9 eV correspond to NaCl and Me-Cl (metal chlorides), respectively. The O 1s spectrum exhibits components at 530.7 eV and 534.1 eV, suggesting that the corrosion product film mainly consists of O^{2-} (oxides) and H_2O (hydrated compounds). Combined with the SEM morphological observations (Fig. 4c), it is evident that a uniform and dense corrosion product layer formed on the surface of the aged sample. EDS mapping (Fig. 4d) further reveals the surface enrichment of Al and O elements, which is consistent with the distribution of $Al_2O_3/Al(OH)_3$ phases detected by XPS.

This mixed oxide/hydroxide phase forms a continuous passivation layer on the surface, effectively inhibiting the penetration of Cl^- ions (such as those in NaCl-containing salt spray environments) [35], thereby retarding the propagation of pitting corrosion. Literature [36] reports that the Al_2O_3 passive film enhances corrosion resistance by blocking direct contact between the corrosive medium and the substrate, while the hygroscopic nature of $Al(OH)_3$ may further stabilize the passivation film [37].

In contrast, the untreated sample (Fig. 4a) shows numerous surface microcracks and porous corrosion products (Fig. 9a). EDS analysis reveals a locally low O content and significant Cl accumulation, indicating an incomplete passive film. As a result, Cl^- ions readily penetrate the matrix through surface defects, accelerating corrosion. Therefore, the aging treatment, by regulating the distribution of precipitates (Fig. 3), facilitates the formation of a uniform passivation layer, ultimately enhancing the corrosion resistance of the composite material.

4. Discussion

To evaluate the impact of different heat treatment processes on corrosion resistance, this study used a confocal microscope to analyze the three-dimensional surface morphology of untreated, solution-treated, and aged samples after varying durations of salt spray testing. The surface morphology of **untreated samples**, shown in Figs. 10, 11, and 12, revealed prominent protrusions and pits that became increasingly pronounced with longer exposure. After 8 days of corrosion, the pit depth was the greatest, indicating a progressive increase in corrosion severity. The pits varied in size, likely caused by the corrosion and spalling of SiC particles [38].

For **solution-treated samples**, the three-dimensional morphology, depicted in Figs. 13, 14, and 15, showed relatively light corrosion after 4 days, with no significant protrusions or pits. However, after 8 days of corrosion, numerous protrusions and pits appeared, displaying an irregular distribution. These anomalies may be attributed to the attachment of corrosion products [39]. Compared to untreated samples, solution-treated samples

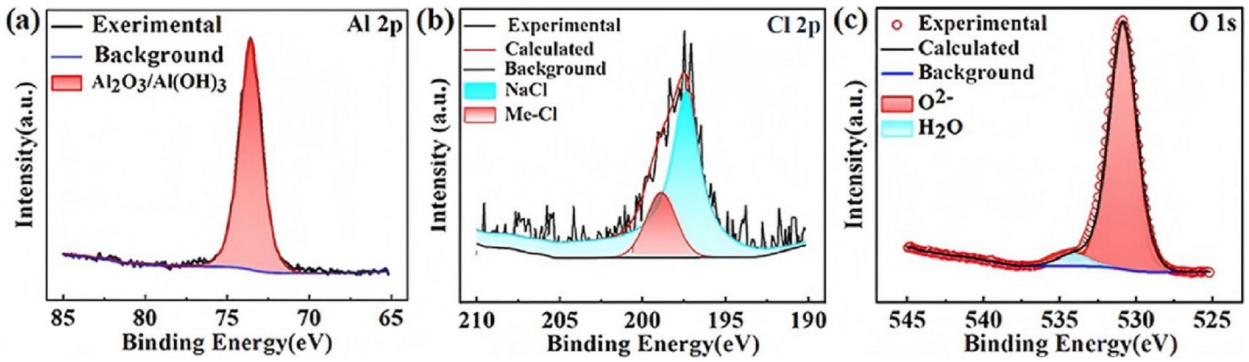

Fig. 9. XPS measurements of Al, Cl, and O on corroded surfaces of aged sample

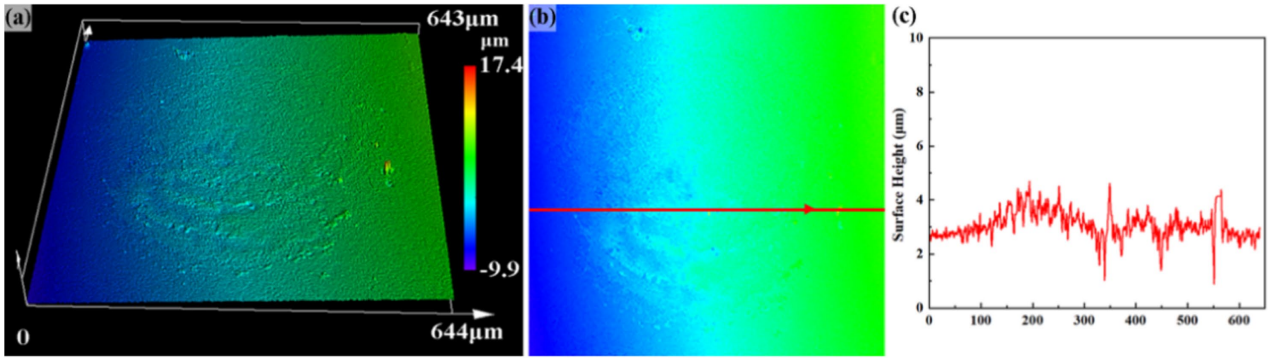

Fig. 10. Confocal micrographs of Untreated sample after 4 d of salt spray corrosion (a) 3D morphology (b) 2D morphology (c) Depth change curve at the red line in Fig. b

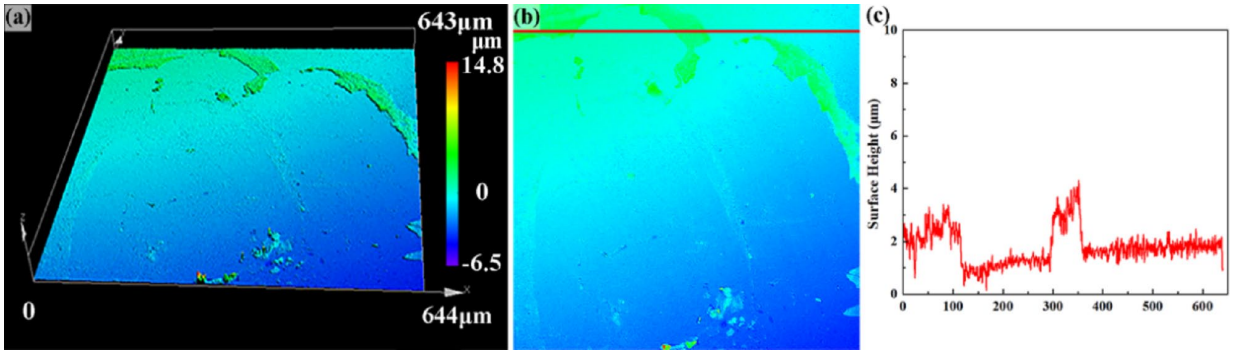

Fig. 11. Confocal micrographs of Untreated sample after 6 d of salt spray corrosion (a) 3D morphology (b) 2D morphology (c) Depth change curve at the red line in Fig. b

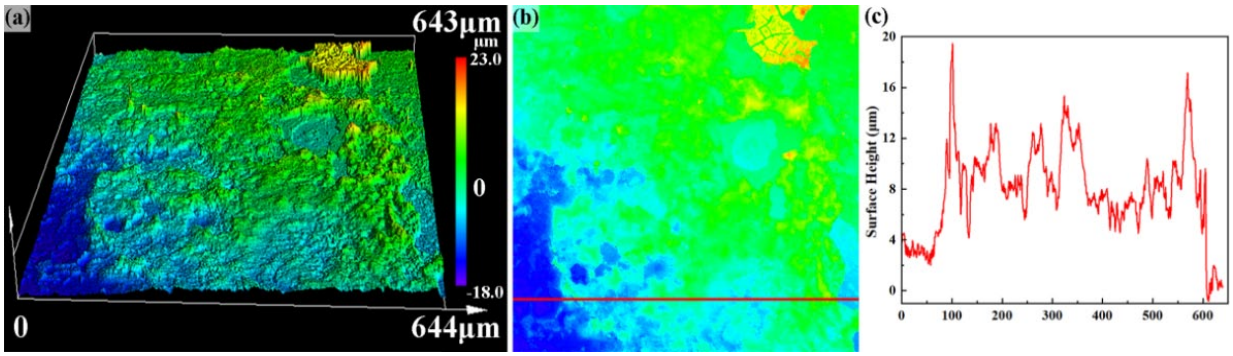

Fig. 12. Confocal micrographs of Untreated sample after 8 d of salt spray corrosion (a) 3D morphology (b) 2D morphology (c) Depth change curve at the red line in Fig. b

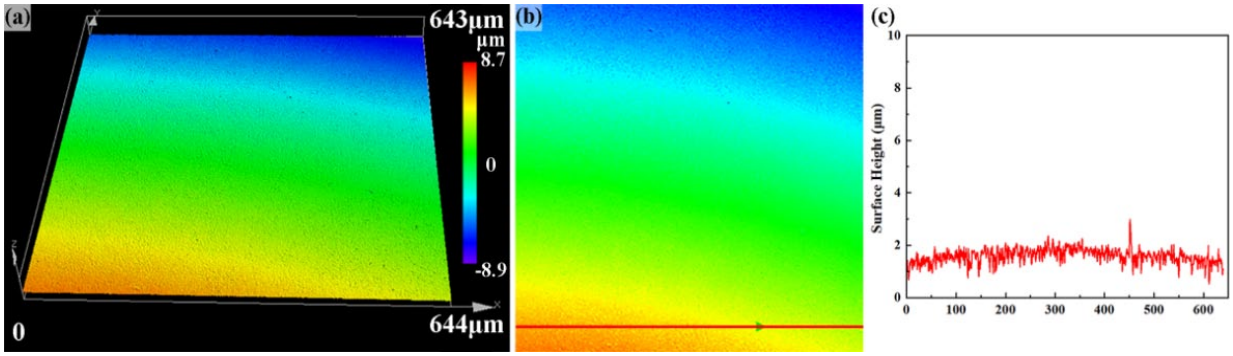

Fig. 13. Confocal micrographs of soild solution sample after 4 d of salt spray corrosion (a) 3D morphology (b) 2D morphology (c) Depth change curve at the red line in Fig. b

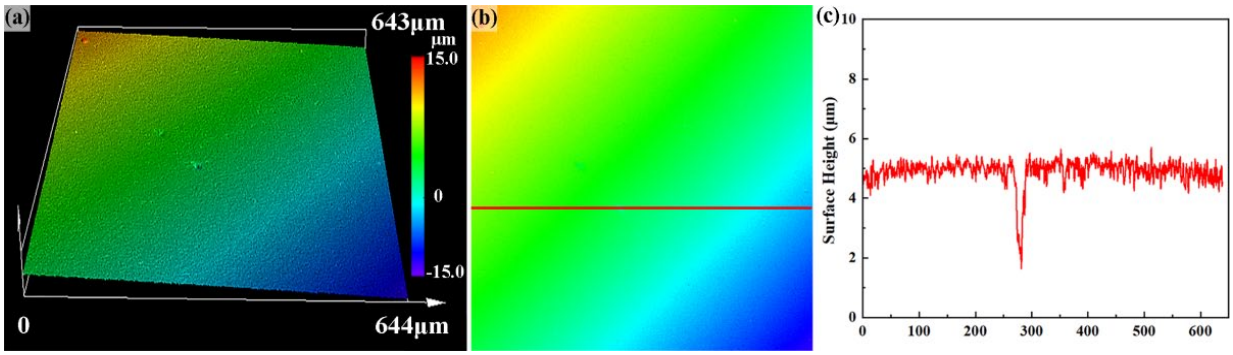

Fig. 14. Confocal micrographs of soild solution sample after 6 d of salt spray corrosion (a) 3D morphology (b) 2D morphology (c) Depth change curve at the red line in Fig. b

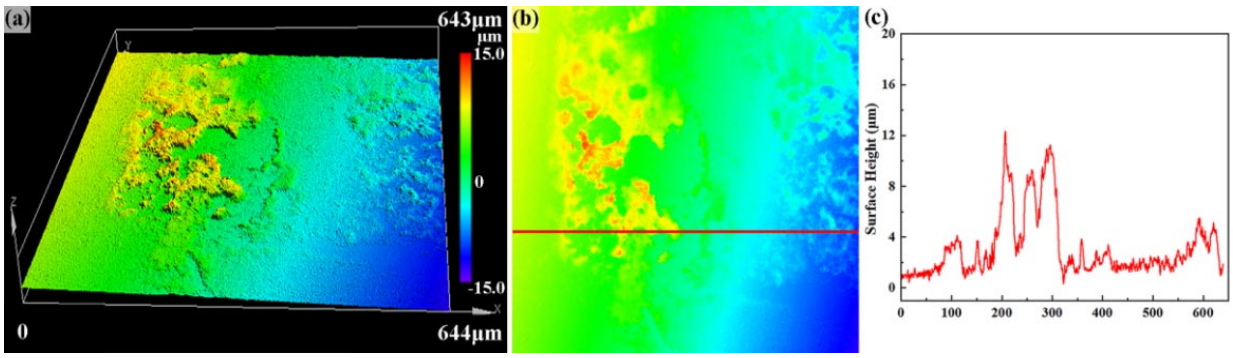

Fig. 15. Confocal micrographs of soild solution sample after 8 d of salt spray corrosion (a) 3D morphology (b) 2D morphology (c) Depth change curve at the red line in Fig. b

exhibited shallower corrosion depths and smaller pitting areas, though both increased with longer exposure times. This analysis highlights that solution treatment reduces the extent and severity of corrosion compared to untreated samples, although the protective effect diminishes with prolonged exposure.

Figs. 16, 17, and 18 show the three-dimensional morphology changes of aged samples after different durations of salt spray testing. After 4 and 6 days of corrosion, the surfaces remain relatively smooth, with no significant protrusions or pits. However, after 8 days, surface undulations become more pronounced, and corrosion depth increases significantly. The deep pits observed are likely caused by the spalling of SiC particles, which expose the underlying matrix and accelerate localized corrosion.

Across untreated, solution-treated, and aged samples, a similar trend is observed: surface undulations increase with extended corrosion time. At 4 days, corrosion marks are minimal. By 6 days, protrusions and pits become more noticeable, and at 8 days, pitting depth and area expand significantly. Untreated samples exhibit the deepest pits and most severe damage, followed by solution-treated samples, with aged samples showing the least damage.

In salt spray corrosion tests, corrosion depth measurements often depend on the definition of the reference plane or zero point, which can vary and cause inconsistencies. To address this, this study utilized variance of surface morphology fluctuations as a more reliable metric, calculated from 100 sampling points

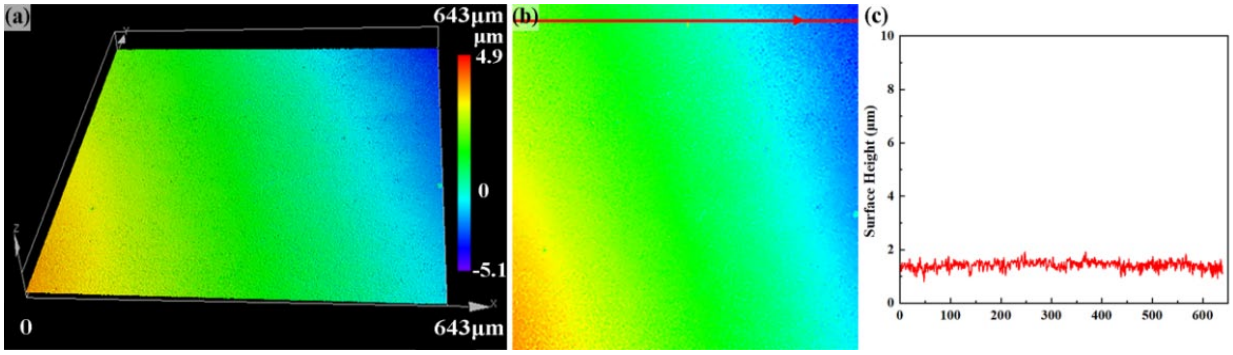

Fig. 16. Confocal micrographs of solution aging sample after 4 d of salt spray corrosion (a) 3D morphology (b) 2D morphology (c) Depth change curve at the red line in Fig. b

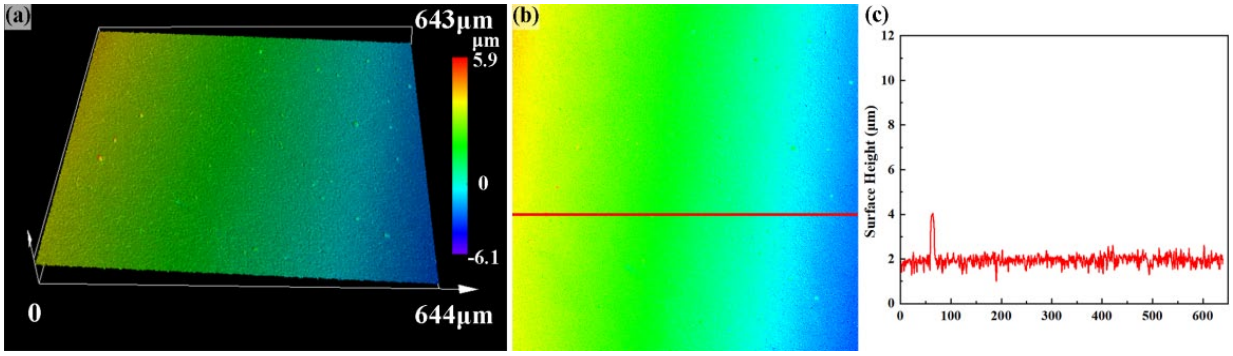

Fig. 17. Confocal micrographs of solution aging sample after 6 d of salt spray corrosion (a) 3D morphology (b) 2D morphology (c) Depth change curve at the red line in Fig. b

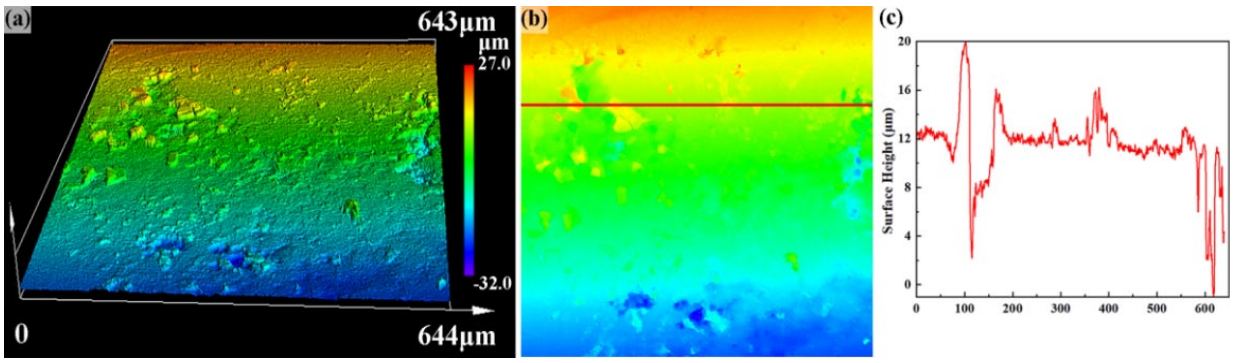

Fig. 18. Confocal micrographs of solution aging sample after 8 d of salt spray corrosion (a) 3D morphology (b) 2D morphology (c) Depth change curve at the red line in Fig. b

on depth variation curves (Fig. 19). Variance is a statistical measure that captures surface roughness, protrusions, and pits, providing a comprehensive description of surface unevenness and microstructural changes caused by corrosion.

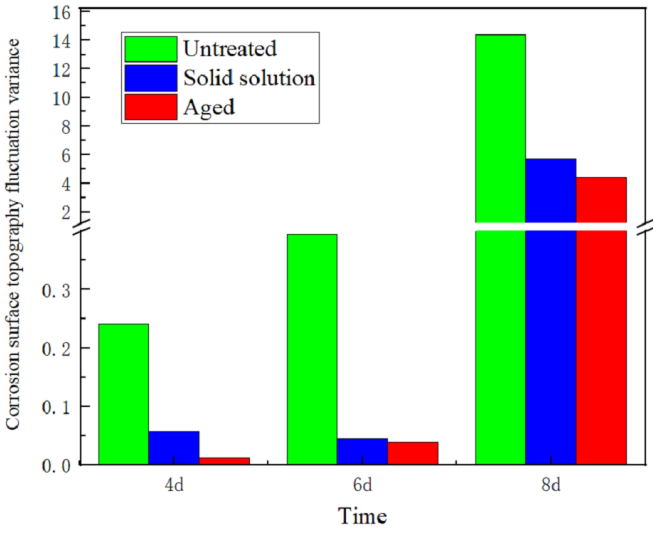

Fig. 19. 4d, 6d, 8d Salt Spray Corrosion Surface Morphology Fluctuation Variance

Compared to depth measurements, variance analysis offers significant advantages by reflecting overall changes in surface morphology and highlighting corrosion heterogeneity and localized damage. As shown in Fig. 19, variance provides a robust and reliable method for evaluating material corrosion resistance, offering a more accurate understanding of the effects of prolonged corrosion on untreated, solution-treated, and aged samples.

As shown in Fig. 19, the variance of surface morphology fluctuations for untreated, solution-treated, and aged samples increases with longer salt spray corrosion times. After 4 days of corrosion, the variances are 0.24, 0.05, and 0.01 for untreated, solution-treated, and aged samples, respectively, indicating relatively minor fluctuations and smooth surface morphology. By 6 days, these values increase to 0.39, 0.04, and 0.03, respectively, with untreated samples showing more significant surface undulations due to lower corrosion resistance. At 8 days, the variances rise significantly to 14.40 for untreated samples, 5.73 for solution-treated samples, and 4.40 for aged samples. The quantitative summary of the corrosion morphology evolution characteristics is presented in TABLE 3, confirming that surface irregularities and corrosion depth are most pronounced in untreated samples and least severe in aged samples.

Relevant literature [40-43] indicates that during the corrosion process, irregularly sized surface pits gradually form, a phenomenon closely related to the corrosion-induced spalling of SiC particles and their electrochemical coupling effect with the aluminum matrix. In a corrosive medium, the aluminum matrix (anode, with lower potential) and SiC particles (cathode, with higher potential) form localized galvanic couples, leading to preferential dissolution of aluminum at the interface and accelerating pitting initiation. The superior corrosion resistance of the aged sample can be attributed to the heat-treatment-induced regulation of $CuMgAl_2$ phase distribution. In both the untreated and solution-treated states, $CuMgAl_2$ tends to agglomerate at grain boundaries or near SiC particles, forming micron-scale enrichment zones. These regions with locally high current density intensify galvanic corrosion. In contrast, aging treatment promotes a uniform dispersion of the $CuMgAl_2$ phase within

TABLE 3

Evolution of corrosion morphology parameters for SiCp/Al-Mg-Si-Cu under different heat treatments

	Untreated			Solution Treated			Aged Treated		
Time	**4 d**	**6 d**	**8 d**	**4 d**	**6 d**	**8 d**	**4 d**	**6 d**	**8 d**
Variance of corrosion surface morphology fluctuations	0.24	0.39	14.40	0.05	0.04	5.73	0.01	0.03	4.40
Average depth	2 μm	4 μm	8 μm	≤1.5 μm	3.2 μm	Irregular pattern	1 μm	1.5 μm	Irregular pattern

the matrix, significantly reducing electrochemical heterogeneity at the interface and suppressing localized corrosion propagation. Combined with corrosion morphology analysis, the uniformly distributed $CuMgAl_2$ phase can effectively retard Cl^- ion penetration paths, thereby synergistically mitigating the nucleation and growth of pitting. As a result, the aged samples exhibit improved long-term stability under corrosive environments.

Electrochemical analysis supports these findings. The corrosion current density (Icorr) for aged samples is the lowest at 1.616×10^{-7} A/cm^2, followed by solution-treated samples at 5.573×10^{-7} A/cm^2 and untreated samples at 1.537×10^{-6} A/cm^2, indicating the poorest corrosion resistance for untreated samples. Electrochemical Impedance Spectroscopy (EIS) reveals that aged samples exhibit the highest charge transfer resistance, reflecting stronger corrosion resistance, while untreated samples show the lowest. XPS analysis further confirms that aged samples feature a dense protective oxide film composed of Al_2O_3/$Al(OH)_3$ and hydroxides, along with chlorides (NaCl and Me-Cl) in the corrosion product film, which effectively block corrosive agents. In contrast, untreated and solution-treated samples lack this protective film, leading to higher corrosion rates.

In summary, the order of corrosion resistance is: aged samples > solution-treated samples > untreated samples. Aging treatment significantly enhances corrosion resistance by improving surface compactness and stability, outperforming both untreated and solution-treated samples, particularly in long-term corrosion processes.

Although the current work clarifies the role of heat treatment in regulating the corrosion-mechanical properties of SiCp/Al-Mg-Si-Cu composites, the impact of cooling strategies during solution treatment remains a critical yet unexplored factor. Variations in cooling rates may significantly alter the precipitation kinetics of intermetallic phases and residual stress distribution at the particle-matrix interface. Future studies should systematically investigate how controlled cooling (e.g., liquid quenching vs. air cooling) modulates the size, dispersion, and interfacial bonding of $CuMgAl_2$ precipitates. Combined with advanced characterization techniques and multi-scale simulations, such efforts could unravel the dynamic interplay between thermal history, microstructural evolution, and corrosion resistance, ultimately guiding the design of composite materials with balanced performance.

5. Conclusions

This study examined the mechanical properties, microstructure, and corrosion resistance of untreated, solution-treated, and aged SiCp/Al-Mg-Si-Cu aluminum matrix composites, By further analyzing the microstructure, corrosion traces, and polarization curves, the following conclusions were drawn:

Aging treatment resulted in the uniform precipitation of $CuMgAl_2$ phases, significantly enhancing material performance. The aged samples achieved a hardness of 134 HV and a tensile strength of 470 MPa, improving both strength and ductility.

With the extension of corrosion time, the phenomenon of particle spalling-induced corrosion on the SiCp/Al-Mg-Si-Cu composite surface became increasingly noticeable. After 8 days of corrosion, the surface morphology variance of untreated, solution-treated, and aged samples were 14.40, 5.73, and 4.40, respectively. Electrochemical test results showed that aged samples exhibited the best corrosion resistance, with a corrosion current density of 1.616×10^{-7} A/cm^2, significantly lower than solution-treated (5.573×10^{-7} A/cm^2) and untreated samples (1.537×10^{-6} A/cm^2). AC impedance spectra showed that aged samples had the largest capacitive arc, indicating higher charge transfer resistance. XPS analysis revealed that finely distributed $CuMgAl_2$ phases effectively blocked corrosive agents and significantly improved anti-corrosion performance.

In summary, heat treatment, particularly aging, significantly enhances the mechanical strength and corrosion resistance of SiCp/Al-Mg-Si-Cu composites, supporting their application in corrosive environments.

Acknowledgments

This work was supported by the Special project for the construction of doctoral teacher studios of Nantong Institute of Technology (No. NIT-WP202404). Yuanji Shi is indebted to the Financial Support from the Qing Lan Project of Jiangsu Province, China.

Conflicts of Interest statement

The author declares that all authors have no conflict of interest.

REFERENCES

[1] K. Kalaiselvan, N. Murugan, S. Parameswaran, Production and characterization of AA6061-B4C stir cast composite. Mater. Des. **32** (7), 4004-4010 (2011).
DOI: https://doi.org/10.1016/j.matdes.2011.03.018

[2] P. Samal, P. RVundavilli, A. Meher, M.M. Mahapatra, Recent progress in aluminum metal matrix composites: A review on processing, mechanical and wear properties. J. Manuf. Process. **59**, 131-152 (2020).
DOI: https://doi.org/10.1016/j.jmapro.2020.09.010

[3] P. Garg, A. Jamwal, D. Kumar, K.K. Sadasivuni, C.M. Hussain, P. Gupta, Advance research progresses in aluminium matrix composites: manufacturing & applications. J. Mater. Res. Technol. **8** (5), 4924-4939 (2019).
DOI: https://doi.org/10.1016/j.jmrt.2019.06.028

[4] J. Suthar, K.M. Patel, Processing issues, machining, and applications of aluminum metal matrix composites. Mater. Manuf. Process. **33** (5), 499-527 (2018).
DOI: https://doi.org/10.1080/10426914.2017.1401713

[5] M.O. Bodunrin, K.K. Alaneme, L.H, Chown. Aluminium matrix hybrid composites: a review of reinforcement philosophies; me-

chanical, corrosion and tribological characteristics. J. Mater. Res. Technol. **4** (4), 434-445 (2015).
DOI: https://doi.org/10.1016/j.jmrt.2015.05.003

[6] S.K. Shaha, Development and Characterization of Cast Modified SI-CU-MG Alloys for Heat Resistant Power Train Applications. PhD thesis, Toronto Metropolitan University, ON M5B 2K3 (2015).

[7] G.N. Ma, S.Z. Zhu, D. Wang, B.L. Xiao, Z.Y. Ma, Aging Behaviors and Mechanical Properties of SiC/A1-Zn-Mg-Cu Composites. Jinshu xuebao. **59** (12), 1655-1664 (2023).
DOI: https://doi.org/10.11900/0412.1961.2021.00473

[8] S.Z. Zhu, G.N. Ma, D. Wang, B.L .Xiao, Z.Y. Ma, Suppressed negative influence of natural aging in SiCp/6092Al composites. Mater. Sci. Eng. A. **767**, 138422 (2019).
DOI: https://doi.org/10.1016/j.msea.2019.138422

[9] S.Z. Zhu, D. Wang, Q.Z. Wang, B.L. Xiao, Z.Y. Ma, Influence of Cu Content on the Negative Effect of Natural Aging in SiC/Al-Mg-Si-Cu Composites. Jinshu xuebao. **57**, 928-36 (2021).
DOI: https://doi.org/10.11900/0412.1961.2020.00330

[10] I.B. Singh, D.P. Mandal, M. Singh, S. Das, Influence of SiC Particles Addition on the Corrosion Behavior of 2014 Al-Cu Alloy in 3.5%wt. NaCl Solution. Corros. Sci. **51** (2), 234-241 (2009).
DOI: https://doi.org/10.1016/j.corsci.2008.11.001

[11] H.M. Zakaria, Microstructural and Corrosion Behavior of Al/SiC Metal Matrix Composites. Ain. Shams. Eng. J. **5** (3), 831-838 (2014). DOI: https://doi.org/10.1016/j.asej.2014.03.003

[12] Y.P. Xiao, Q.L. Pan, W.B. Li, X.Y. Liu, Y.B. He, Influence of heat treatment on corrosion behaviour of Al-Zn-Mg-Cu-Zr-Sc alloy. Werkst Korros. **63** (5), 421-430 (2012).
DOI: https://doi.org/10.1002/maco.201005923

[13] Y. Xie, X. Meng, D. Mao, Z. Qin, L. Wan, Y. Huang, Homogeneously dispersed graphene nanoplatelets as long-term corrosion inhibitors for aluminum matrix composites. ACS Appl. Mater. Interfaces **13** (27), 32161-32174 (2021).
DOI: https://doi.org/10.1021/acsami.1c07148

[14] M. Suśniak, J. Karwan-Baczewska, J. dutkiewicz, M. Actis Grande, M. Rosso, An experimental study of aluminum alloy matrix composite reinforced sic made by hot pressing method. Arch. Metall. Mater. **60**, 1523-7 (2015).
DOI: https://doi.org/10.1515/amm-2015-0165

[15] C.H. Mao, X.D. Sun, Q.S. Liang, J. Yang, D, The Corrosion Mechanism of WCp/2024Al Matrix Composites. Jun. Corros. Prot. **33** (01), 32-35 (2012).
DOI: https://doi.org/10.1007/s12598-013-0116-z

[16] Y.M. Han, X.G. Chen, Electrochemical behavior of Al-B4C metal matrix composites in NaCl solution. Materials **8** (9), 6455-6470 (2015). DOI: https://doi.org/10.3390/ma8095314

[17] J.H. Aval, Effects of aging heat treatment on microstructure and corrosion behavior of friction surfacing treated Al-Zn-Mg-Cu matrix composite. T. Nonferr. Metal. Soc. **33** (08), 2303-2313 (2023). DOI: https://doi.org/10.1016/S1003-6326(23)66260-0

[18] N.M.S. Kumar, G.K. Pramod, P. Samrat, M. Sadashiva, A critical review on heat treatment of aluminium alloys. Mater. Today. **58**, 71-79 (2022).
DOI: https://doi.org/10.1016/j.matpr.2021.12.586

[19] P. Wang, C. Gammer, F. Brenne, T. Niendorf, J. Eckert, S. Scudino, A heat treatable TiB_2/Al-3.5 Cu-1.5 Mg-1Si composite fabricated by selective laser melting: Microstructure, heat treatment and mechanical properties. Compos. B Eng. **147**, 162-168 (2018).
DOI: https://doi.org/10.1016/j.compositesb.2018.04.026

[20] K.V. Yang, P. Rometsch, C.H.J. Davies, A.J. Huang, X.H. Wu, Effect of heat treatment on the microstructure and anisotropy in mechanical properties of A357 alloy produced by selective laser melting. Mater. Des. **154**, 275-290 (2018).
DOI: https://doi.org/10.1016/j.matdes.2018.05.026

[21] Z.Z. Duan, Z.Y. You, A.X. Jiang, G.P. Qiao, T. Liu, X.S. Zhao, Effect of Heat Treatment on the Microstructure and Properties of Extrusion-Cast SiCp/ZL101 Aluminum Matrix Composites. Spec. Cast. Nonferrous Aloys **41** (06), 684-688 (2021).
DOI: https://doi.org/10.15980/j.tzzz.2021.06.005

[22] L.F. Wang, J. Sun, X.L. Yu, Y. Shi, X.G. Zhu, L.Y. Cheng, H.H. Liang, B. Yan, L.J. Guo, Enhancement in mechanical properties of selectively laser-melted AlSi10Mg aluminum alloys by T6-like heat treatment. Mat. Sci. Eng. A. **734**, 299-310 (2018).
DOI: https://doi.org/10.1016/j.msea.2018.07.103

[23] X. Zhang, T. Chen, Simultaneously enhancing the strength and ductility of particulate-reinforced aluminum matrix composite by aging treatment. JMaterRes. **36**, 3445-59 (2021).
DOI: https://doi.org/10.1557/s43578-021-00389-x

[24] G.P. Lei, B. Wang, J. Lu, C. Wang, Y. Li, F. Luo, Effects of solid solution temperature on the microstructure and properties of 6013 aluminum alloy. Mater. Chem. Phys. **280**, 125829 (2022).
DOI: https://doi.org/10.1016/j.matchemphys.2022.125829

[25] P. Liu, J.Y. Hu, H.X. Li, S. Sun, Y. Zhang, Effect of heat treatment on microstructure, hardness and corrosion resistance of 7075 Al alloys fabricated by SLM. J. Manuf. Process. **60**, 578-585 (2020).
DOI: https://doi.org/10.1016/j.jmapro.2020.10.071

[26] D. Ghanbari, M.K. Asgarani, K. Amini, Influence of heat treatment on mechanical properties and microstructure of the Al2024/SiC composite produced by multi–pass friction stir processing. Measurement. **104**, 151-158 (2017).
DOI: https://doi.org/10.1016/j.measurement.2017.03.024

[27] S. Bharti, N.D. Ghetiya, V. Dutta, Investigating microhardness and wear behavior of Al5052/ZrO2 surface composite produced by friction stir processing. Mater. Today. **44**, 52-57 (2021).
DOI: https://doi.org/10.1016/j.matpr.2020.06.318

[28] A. Shafiei-Zarghani, S.F. Kashani-Bozorg, A. Zarei-Hanzaki, Microstructures and mechanical properties of Al/Al2O3 surface nano-composite layer produced by friction stir processing. Mater. Sci. Eng. A Struct. Mater. **500**, 84-91 (2009).
DOI: https://doi.org/10.1016/j.msea.2008.09.064

[29] R.A. Kumar, K. Rajan, T. Amit, A.S. Yadav, Effect of Microstructure on Mechanical Behaviors of Al6061 Metal Matrix Composite Reinforced with Silicon Nitride (Si3N4) and Silicon Carbide (SiC) Micro Particles. Silicon-Neth., **15** (14), 5911-5923 (2023).
DOI: https://doi.org/10.1007/s12633-023-02468-6

[30] R. Yamanoğlu, E. Karakulak, A. Zeren, M. Zeren, Effect of heat treatment on the tribological properties of Al-Cu-Mg/nano SiC composites. Mater. Design. **49**, 820-825 (2013).
DOI: https://doi.org/10.1016/j.matdes.2013.02.026

[31] P.D. Myriounis, T.S. Hasan, E.T. Matikas, Heat Treatment and Interface Effects on the Mechanical Behavior of SiC-Particle Reinforced Aluminium Matrix Composites. J. ASTM Int. **5** (7), 1-10 (2008).
DOI: https://dx.doi.org/10.1520/JAI101624

[32] Z.Y. Tang, Q.Y. Xing, S.J. Yang, N. Ding, Hot Deformation Behavior of Novel Al-Zn-Mg-Sc-Er-Zr Alloy. J. Mater. Eng. Perform. **50** (03), 131-137 (2022).
DOI: https://doi.org/10.11868/j.issn.1001-4381.2021.000319

[33] U. S. Ikele, K. K. Alaneme, A. Oyetunji, Corrosion and wear behaviours of aluminium composites reinforced with palm kernel shell ash and silicon carbide. T. Indian I. Metals **76** (3), 765-76 (2023).
DOI: https://doi.org/10.1007/s12666-022-02760-w

[34] M. Karthikraja, K. Ramanathan, K.T. Loganathan, S. Selvaraj, Corrosion behaviour of SiC and Al2O3 reinforced Al 7075 hybrid aluminium matrix composites by weight loss and electrochemical methods. J. Indian Chem. Soc. **100** (5), 101002 (2023).
DOI: https://doi.org/10.1016/j.jics.2023.101002

[35] L.F. Xie, W.L. Zhou, Salt spray corrosion behavior and pitting resistance of Ti-15V-3Cr-3Al-3Sn alloy evaluated using XPS, SKPFM, and electrochemical technique. J. Solid State Electrochem. **26** (8), 1585-1603 (2022).
DOI: https://doi.org/10.1007/s10008-022-05193-z

[36] H. Feng, Z. Jiang, H. Li, P. Lu, S. Zhang, H. Zhu, B. Zhang, T. Zhang, D. Xu, Z. Chen, Influence of nitrogen on corrosion behaviour of high nitrogen martensitic stainless steels manufactured by pressurized metallurgy. Corros. Sci. **144**, 288-300 (2018).
DOI: https://doi.org/10.1016/j.corsci.2018.09.002

[37] S. Ningshen, M. Sakairi, K. Suzuki, S. Ukai, The corrosion resistance and passive film compositions of 12% Cr and 15% Cr oxide dispersion strengthened steels in nitric acid media. Corros. Sci. **78**, 322-334 (2014).
DOI: https://doi.org/10.1016/j.corsci.2013.10.015

[38] A.H. Karabacak, A. Çanakçı, F. Erdemir, S. Özkaya, M. Çelebi, Corrosion and Mechanical Properties of Novel AA2024 Matrix Hybrid Nanocomposites Reinforced with B4C and SiC Particles. Silicon-Neth. 1-13 (2022).
DOI:https://doi.org/10.1007/s12633-021-01582-7

[39] I. Gurrappa, B.V.V. Prasad, Corrosion characteristics of aluminium based metal matrix composites. J. Mater. Sci. Technol. **22** (1), 115-122 (2013).
DOI: https://doi.org/10.1179/174328406X79324

[40] X.P. Ding, Q. Zhang, Y.Y. Zhou, Y.Q. Guo, M. Tang, Y. Gong, Corrosion and Wear Resistance of Alloy and SiC/AlSi10Mg Composite Materials. Cailiao Gongcheng. **52** (10), 97-105 (2024).
DOI: https://doi.org/10.11868/j.issn.1001-4381.2023.000435

[41] X.J. Xu, Y. Luo, Y.K. Zhang, T. Sao, Z.Q. Zhang, F.B. Zhang, G.C. Wu, Y. Wao, The Effect of Strengthening Solution Treatment on the Corrosion Performance of Sr-Sc 7085 Aluminum Alloy. J. Mater. Heat .Treat. **33** (11), 28-32 (2012).
DOI: CNKI:SUN:JSCL.0.2012-11-007

[42] S.A. Zakaria, A.S. Anasyida, H. Zuhailawati, B.K. Dhindaw, N.A. Jabit, A. Ismail, Characterization of mechanical and corrosion properties of cryorolled Al 1100 alloy: Effect of annealing and solution treatment. T. Nonferr. Metal. Soc. **31** (10), 2949-2961 (2021). DOI: https://doi.org/10.1016/S1003-6326(21)65705-9

[43] S.H. Pan, J. Yuan, M.P. Moodispaw, C. Linsley, J.K. Liu, A.A. Luo, T. Alan, X.C. Li, Corrosion performance of nano-treated aluminum alloy A206 with TiC nanoparticles. Werkst. Korros. **74** (3), 419-429 (2023).
DOI: https://doi.org/10.1002/maco.202213503